On the indentation size effect in spherical indentation.

Ian Spary, Andy Bushby, Nigel M. Jennett

On the indentation size effect in spherical indentation.

Journal:	*Philosophical Magazine & Philosophical Magazine Letters*
Manuscript ID:	TPHM-06-Mar-0068.R2
Journal Selection:	Philosophical Magazine
Date Submitted by the Author:	07-Jun-2006
Complete List of Authors:	Spary, Ian; Queen Mary, University of London, Materials Bushby, Andy; Queen Mary, University of London, Materials Jennett, Nigel; National Physical Laboratory, Materials Performance; National Physical Laboratory, Materials Performance
Keywords:	finite-element modelling, indentation, stress-strain measurements
Keywords (user supplied):	indentation stress -strain, size effect

On the indentation size effect in spherical indentation.

I.J. SPARY [1], A.J. BUSHBY [1*] and N.M.JENNETT[2]

[1]Department of Materials, Queen Mary, University of London, Mile End Road, London, E1 4NS, UK, Phone: +44 (0) 20 7882 5150, Fax: +44 (0) 20 8981 9804, Ext 5276, Email: a.j.bushby@qmul.ac.uk / Ext 7418, Email: i.spary@qmul.ac.uk

[2] Materials Performance, National Physical Laboratory, Hampton Road , Teddington, Middlesex, TW11 0LW, UK Phone: +44 (0) 20 8943 6641, Fax: +44 (0) 20 8614 0451, Email: nigel.jennett@npl.co.uk

* Corresponding Author: Email: a.j.bushby@qmul.ac.uk

Philosophical Magazine
Special Issue: Instrumented Indentation

Size effects in plasticity at small length scales have been widely reported in a variety of loading situations. The hardness size effect has often been cited as an archetypal example. The indentation size effect was clearly demonstrated by Lim and Chaudhri (1999) in spherical indentation experiments on Copper and subsequently in experiments on Iridium by Swadener *et al*, (2002). They showed that large radius indenters produced an indentation stress-strain curve independent of indenter radius with a hardening coefficient equivalent to that in uniaxial tests on the same materials. For smaller indenters the indentation stress-strain curves appeared at progressively higher pressures for smaller radius indenters. Here we present similar experimental data for Nickel. We simulate these experiments by inputting the uniaxial stress-strain data into a finite element model, which has no intrinsic length scale dependence (essentially using the von Mises criterion for yield). We show that a simple increase in the initial yield stress of the uniaxial stress-strain curve input to the model, allows the indentation behaviour of the smaller radius indenters to be simulated. The increase in yield stress with decreasing indenter radius is shown to follow a single relation for all the metals studied; Al, Cu, Ni, and Ir. We show that the indentation size effect is a geometrical effect; consistent with critical thickness theory for the initiation of yielding over a finite volume. The magnitude of the size effect depends only on indenter radius, providing a predictive method for the yield strength in spherical nanoindentation of bulk materials.

Deleted:

Comment [A1]:

Keywords:

Spherical indentation, size effect, indentation stress-strain, finite element modelling

1. Introduction

Indentation size effects have been observed since the early days of indentation testing [1]. In many cases, this effect is largely due to the rising uncertainties involved in making and measuring small indentations. In particular the poorly defined tip shape of Vickers indenters at low indentation depths is a cause of hardness calculation errors. The advent of instrumented nanoindentation equipment using both greatly improved force and depth resolution and directly calibrated tip geometries, has largely removed this source of error [2,3] revealing a residual indentation size effect that has a real physical basis [4]. For pointed indenters, of fixed geometry, i.e. Berkovich, Vickers and cones, the force applied to the projected area of contact (hardness) is seen to decrease as the depth of indentation increases. There are many examples in the literature of this phenomenon, especially the classic data of Nix and Gao [5]. For these indenter geometries there is significant plastic flow from an early stage in the indentation cycle. Many attempts to explain the phenomena in terms of plastic flow behaviour have been reported, particularly using the theory of strain gradient plasticity [5]. Other studies have considered the influence of surface oxide films and strain rate effects [6,7]. Indentation size effects have also been reported for the spherical indenter geometry [8-11]. In this case, plastic flow is not necessarily induced from the start of contact and the contact geometry changes during the indentation cycle, generating the so called 'indentation stress-strain curve'. Tabor [1] showed that for a given metal the indentation stress-strain curve was independent of ball size, for large radius indenters. Furthermore, Tabor showed that the shape of the indentation stress-strain curve was analogous to the uniaxial stress-strain curve from a tensile test when plotted as $P_m/2.8$ against $0.2a/R$. There

is currently a resurgence of interest in this idea with the aim of predicting tensile stress-strain properties from a non-destructive indentation test. Such an approach would be of great benefit to critical industries such as oil and gas production and power generation. However, a thorough appreciation of indentation size effects is required to achieve this aim successfully. Recently, several studies have shown that for smaller radius spherical indenters (say, $R < 200\mu m$) the indentation stress-strain curve moves to increasingly higher pressures for indenters with smaller radii [8-11]. For spherical indenters the size effect is more pronounced and is dependent on the ball size, rather than the depth of indentation. Lim *et al* [8-9] showed the size effect in polycrystalline and single crystal annealed Copper, the archetypal ductile metal. Swadener *et al* [11], showed a similar behaviour in Iridium, a strong metal with a high shear modulus.

In this paper we build on those studies by comparing the uniaxial stress-strain behaviour to the indentation behaviour for a series of ductile metals by simulation in a finite element model. We show that it is possible to reproduce the size effect seen with small radius indenters by an increase in the initial yield stress. That is, it appears to be more difficult to initiate plasticity within the steep elastic strain gradient beneath a small spherical indenter. Furthermore, the factor by which the yield stress appears to increase scales with the indenter radius in the same way for all the metals tested. The phenomena of an increasing initial yield stress with decreasing indenter radius has been reported before for semiconductor materials, which have a sufficiently high yield stress that the effect can be clearly observed, in spite of the phenomena of 'pop-in' [4,12]. The concept of size dependent yield behaviour is well known in such materials in which coherently strained layers are grown in hetero-epitaxial crystal growth [13,14]. Recently, it has been shown that the same concepts can be used to explain the size effects seen in the flexure of thin foils and the twisting of thin wires

[15]. It might be expected, therefore, that a similar behaviour should be apparent in the complex three dimensional strain gradients beneath an indentation.

2. Methods and Materials

2.1 Experimental approach

Our approach is to re-examine published data on spherical indentation of annealed face centred cubic metals, Cu [8,9], Al [10] and Ir [11]. To this we add new experimental data on Ni to broaden the material property range studied. The material properties of the samples are listed in Table 1.

[Insert Table 1 about here]

In all cases, the basis of the method is the same. Indentation experiments were performed on the polished and annealed surfaces of the metal using a range of indenter sizes from several hundred microns in radius to a few microns in radius. The actual contact area of each indent was measured directly after indentation and the indentation stress and indentation strain calculated as:

$$P_m = \frac{P}{\pi a^2} \qquad (1)$$

and

$$\frac{a}{R} \qquad (2)$$

respectively, where P is the indentation load, a is the radius of the circle of contact between the surface and indenter, and R is the radius of the indenter. This method determines the true projected contact area, independent of any 'pile-up' or 'sink-in' of the contact [8]. Uniaxial mechanical properties were also determined on the same materials in compression or tension.

The methods used to study each material have already been described elsewhere [8-11] but briefly:- For the Al and Cu, the uniaxial data were determined from well lubricated compression of low aspect ratio cylinders. The plastic strain was determined by incrementally compressing the cylinder, unloading and measuring the length of the plastically deformed cylinder. Indenter contact areas were determined by optical microscopy for macroscopic indenters (>100μm radius) and by scanning probe microscopy for smaller radius indenters to an accuracy of about 7%. It should be noted, however, that for macro indentation the edge of the circle of contact was not always clearly defined since the change in optical contrast may be associated with pile-up rather than the true edge of contact. For the Ir the uniaxial data were determined from tensile tests and, in general, the contact areas were calculated from the depth of penetration under load and residual impression depths. Some of these were subsequently checked by optical or scanning probe techniques and the measurements found to be with ±7% for R < 122μm and 10-20% smaller than the contact depth method for the R = 318μm indenter.

2.2 New experiments

The new experiments on Ni were performed in a similar manner. Uniaxial compression tests were performed on an Instron 8511 servo-hydraulic testing frame. Strain gauges recorded strain levels up to 3% plastic strain (TML FLA-1-11) and crosshead movement beyond 3% plastic strain. All indent contact areas were measured by optical microscopy (Olympus BX 60) for macroscopic indenters (> 100μm radius) and by metrological scanning probe microscopy (Park Autoprobe M5, Veeco Instuments, Passadena, CA) for smaller radius indenters to an accuracy of about 3%.

2.3 Finite element modelling

Finite element (FE) modelling was used to simulate the indentation process. The model chosen was a two-dimensional axisymmetric model and was executed using ABAQUS™ finite element code (ABAQUS Inc., Pawtucket, RI), which is a general purpose finite-element program. A rigid ball indenter was modelled and pressed on to the surface of the model, which consisted of a deformable mesh (type CAX4 elements). There was significant refinement of the model towards the surface and in the region of contact and the mesh was surrounded by semi-infinite elements (type CINAX4 elements) to simulate the far-field displacements. The model was constrained to move only in the vertical direction along the axis of symmetry. The indenter was modelled as a rigid spherical surface, to simulate the high elastic modulus indenters used in the experiment, to which a point load was applied. The contact area was calculated under load from the last node in contact (CAREA) and the projected area of contact calculated from geometry. In the experiments, the projected area of contact was measured after complete unloading. It was assumed that elastic recovery of the

indentation on unloading occurs vertically and that any lateral (in plane) recovery is negligible. The model was calibrated by simulating elastic indentation for known material parameters and comparing to Hertzian theory. It was found that there was quantisation noise associated with the contact moving from node to node. An algorithm was used by which the position within the noise that agreed with Hertzian theory was taken as the true contact point.

In the elastic-plastic model, the test material was defined by three sets of parameters: The elastic modulus and Poisson's ratio; The yield stress for the onset of plastic deformation (elastic limit); The plastic true strain as a function of true stress greater than the elastic limit, which was entered into the model in tabular form. These values were obtained directly from the uniaxial testing data and from known values for the elastic constants. The plasticity model used by ABAQUS™ for this simulation was the von Mises yield criterion, which has no intrinsic length scale dependency.

3. Results

The results of indentation experiments (large open symbols) are presented in Figure 1a-d for Al, Cu, Ni and Ir respectively, together with the finite element simulation (small solid symbols) and uniaxial data (solid lines). The Hertzian elastic response is shown as the dashed line. The form of the uniaxial data is represented on the plots using the empirical Tabor relation, such that the uniaxial stress is $P_m/2.8$ and the uniaxial strain is $0.2a/R$. The FE simulation of indentation using the uniaxial data directly in the model is represented by the crosses. Clearly the Tabor relation gives a good representation of the macro indentation data for Cu but is not universal.

Deleted: ¶

[Insert Figure 1 a-d about here, preferably on facing pages]

Entering the uniaxial data directly into the FE model only reproduced the macroscopic ball indentation data for the case of Cu. The elastic limit for Cu is very low and not clearly defined but is of the order of 10MPa, so that the entire uniaxial curve is essentially plastic flow. For this case the Tabor relation follows the macroscopic ball indentation. For the other metals entering the uniaxial data directly in the model did not simulate the macroscopic ball indentation data directly, as shown in Figure 1d for Ir, but tended to underestimate the indentation pressure. For Ni and Ir the yield occurs at significantly higher stress; of the order of 100MPa. However, the elastic limit is still not well defined. Changing the dimensions of the indenter in the model did not reproduce the size effect seen in the indentation experiments for the small radius indenters. This is not surprising since the model uses conventional plasticity theory, which has no intrinsic length scale. Changing the work hardening exponent of the material did not reproduce the size effect.

Deleted: ¶

It was found that the size effect could be simulated by a simple increase in the value of uniaxial yield stress (elastic limit) used in the model. The plastic part of the uniaxial stress–strain curve was translated up the elastic line by an offset (initial yield stress offset). That is, the uniaxial flow curve occurs at higher stress and strain but with the same work hardening rate [16]. The magnitude of the yield stress required to simulate the size effect for each indenter was found from the simulation that gave a best fit to the experimental data. Values for the yield stress are given in Table 2 together with an estimate of the range of yield stress values that might be considered a good fit to the data points. The variation from metal to metal in the precision to which a fit could be made to the data was due partly to the different methods adopted by the different laboratories and partly to scatter between the experimental data points. The data for Iridium has the highest uncertainties due to the low number of data points. This is compounded by the restriction to low values of a/R, due in part

to the thickness of the sample. For the large radius indenters the level of precision to which the yield stress could be determined was of the order of 30%, reducing to less than 10% for the smallest radius indenters. For large radius indenters, the insensitivity of the fit to the (low) values of yield stress contributes strongly to the increased uncertainty.

[Insert Table 2 about here]

The four metals used in this study include a wide range of uniaxial yield strength. However, it should be noted that the all have similar values of yield strain; within a factor of 3. Although the actual values of the elastic limit varied by an order of magnitude for different metals, it was found that the ratio of the yield stress used in the simulation to the uniaxial yield stress, σ_y / σ_0, scaled more closely with the indenter radius as $1/R^{1/3}$, for all metals studied, Figure 2a, than with $1/R^{1/2}$, Figure 2b.

[Insert Figure 2a & 2b about here, preferably on the same page]

4. Discussion

The experimental data in this paper are drawn from several studies in three different laboratories but all using essentially the same methodology. The direct measurement of contact area eliminates much of the error associated with pile-up or sink-in of material around the indentation, as demonstrated by Lim and Chaudhri [8]. However, there remains an uncertainty in defining the edge of contact and the fact that the indentations are not perfectly circular. These factors are increased for shallow indents, that is at low values of

a/R. The measurement uncertainty in contact radius, *a*, results in greater uncertainty in P_m than in *a/R*, as illustrated in Figure 1d for Ir. A similar level of uncertainty is expected in the data for Al, Cu and Ni, Figures 1a-c respectively. In all cases, however, the size effect is clearly demonstrated in the experimental data for metals with a wide range of properties, notwithstanding the experimental uncertainties. There is a similar phenomenon in the finite element model, at low values of *a/R* there are few nodes in contact with the indenter surface, leading to increased uncertainty in the area of contact.

Directly inputting the uniaxial data into the FE model reproduced the empirical Tabor representation of uniaxial data on the indentation stress-strain plot, within the scatter of both experimental data and simulation. However, in most cases the macroscopic ball indentation experimental data did not follow the same relation but appeared at higher values of P_m, implying that a size effect may already be operating for these indenter sizes. This is particularly clear in the Ir data, in which the two largest indenter radii (R = 318μm and R = 1600μm) clearly lie on a similar curve, while the Tabor representation of the uniaxial data lie below, as pointed out by Swadener *et al* [11]. The Tabor relation uses the flow stress for the metal, which is well defined in spite of the fact that the elastic limit is not well defined. For the Al and Cu the uniaxial data is essential all plastic flow. Spherical indentation may well be more sensitive to the initial yield stress since a relative large volume beneath the indentation is at low plastic strain, compared to the small volume at high plastic strain. For pointed indenters a larger proportion of the volume is at high plastic strain and this may contribute to the indentation size effect being more pronounced for spherical indenters.

It was possible for the model to simulate the size effect by a simple increasing the initial yield stress above that of the uniaxial data, implying that the metals appear genuinely stronger. Changing the rate of hardening in the constitutive relation did not reproduce the size effect. The amount of increase in yield stress required to simulate the experimental data

for the smallest radius indenters was significant (an increase of 7.5× for the 5μm radius indenter on Ni) so much so that the values of yield stress used became quite sensitive for the small radius indenters. Thus, despite there being uncertainty in both the experimental data and the FE simulation, as discussed above, the amount of increase in yield stress required is still very significant.

Although the actual values of yield stress vary by an order of magnitude across the range of metals investigated here, as shown in Table 2, it was found that the proportional increase in yield stress with indenter radius was similar in all cases. A linear relation that gave the best fit was found between the normalised yield strength for all the metals and the inverse cube root of indenter radius, Figure 2a. This was not expected. A relation proportional to the inverse square root of indenter radius might be expected from strain gradient plasticity theory, Figure 2b. By definition the intercept on the ordinate must be at a value of 1 (solid lines). The fit through the data for indenters of R< 30μm, with the least uncertainty, when not constrained to intercept at 1 (dashed lines) is seen to intercept close to one in Figure 2a but at an unphysical value of about 3 in Figure 2b. The abscissa of Figure 2 covers over two orders of magnitude in indenter radius. The fact that a common relation is obtained for a wide range of indenter radius and a wide range of material properties, Table 1, suggests that the effect is dominated by the geometry of the stress field beneath a spherical indenter. Swadener *et al* [11] argued that the size effect in Ir could be explained by strain gradient plasticity, by using four constants in their calculation. Recently, Qu *et al* [17] have also generated a strain gradient plasticity model using finite element methods. Their model was based on a strain gradient plasticity theory [18] established from the Taylor dislocation model and fits the Ir data quite well at significant plastic strain but rather less well at low strain and does not reproduce the data for the 14μm radius indenter tip. Lim and Chaudhri

[8], however, showed that strain gradient plasticity could not explain the size effect in Copper and suggested that homogeneous nucleation of dislocations provided an explanation for the size effect. There has been considerable debate within the mechanics community over recent years as to whether plasticity size effects are the result of dislocation interaction events or dislocation generation events. There is an increasing amount of evidence that dislocation generation becomes more difficult when strain is distributed over a small volume; that volume being defined either by restricted physical dimensions or by the width of a strain energy distribution. Such geometrical effects on the onset of plastic deformation are well established in critical thickness theory [13-15] and experimentally verified in the large literature on growth of strained layers. They have been observed experimentally in indentation of crystals [12] and patterned lines [19], micropillar compression [20] and microflexure [21] experiments. An emerging opinion is that at lengths scales of the order of microns, strain gradient plasticity models can be fitted to the observed size effects well, that is, dislocation interaction dominates. At smaller length scales the size effects become dominated by the increased difficulty to generate dislocations [22, 23]. Yield in restricted volumes has been shown to be size dependent in both theory [24] and in atomistic modelling [25]. Gerberich *et al* [26] approached the indentation size effect via an energy balance argument based on the observations of Horstemeyer and Baskes [25] of a surface area to volume ratio of the plastic deformation. A wide range of metals were found to obey a relationship, in the nanoindentation range, of the form $H/\sigma_o \propto 1/R^{1/3}$. Although this result is based on a very different methodology and theoretical consideration, it bares a remarkable similarity to our Figure 2a. We do not attempt to formalise the comparison between the current work and that of ref[26] here but simply demonstrate that the observed size effect in spherical indentation can be explained by a restriction on dislocation generation as the volume of strained material (defined by the width of the strain energy distribution beneath

the indenter) is reduced. Such a mechanism does not predict any changes to plastic flow, except that it occurs at elevated stress levels.

An increasing elastic limit with decreasing indenter radius has been clearly observed in InGaAs alloys, which possess very high hardness, where the elastic portion of the curve is significant and the departure from elastic to plastic behaviour is clear [4, 12]. However, in those materials the uniaxial tensile properties cannot be determined in the same way as the experiments examined here. Furthermore, macroscopic ball indentation tests cannot be performed because of the problem of Hertzian cracking before the yield point is reached. Such yield phenomena cannot be explained by strain gradient plasticity, since at the elastic limit there is no plastic strain gradient. The generation of a dislocation is a cooperative process involving many atoms in the crystal and this process is necessarily finite (or quantized) rather than continuous. The increase in the elastic limit is consistent with the argument that as an imposed elastic strain becomes increasingly localised, a higher force will be required to satisfy the energetic yield criteria when integrated over the effective volume of material affected by the generation of a dislocation. This concept has been applied to the 2 dimensional strain gradients in thin beams in flexure where an apparent increase in the initial yield stress is also anticipated [15]. The increase in yield strength for thinner beams has recently been demonstrated experimentally [21]. A similar mechanism might be expected to operate in the 3 dimensional strain gradients beneath an indentation. Furthermore, if any dimension of a material compromises the effective volume of yield, then a further enhancement of yield stress should be expected. Such a phenomenon has been observed for ductile coatings on an effectively rigid substrate [27]. For pointed indenters with a spherical tip defect and constant included angle, the initial response should be similar to a small spherical indenter, with an enhanced yield stress. The hardness will then decline as the depth of indentation increases once self similarity of contact (constant indentation strain i.e. a/R) is

reached. Therefore, the magnitude of the size effect would depend on the sharpness of the tip; an extremely sharp tip showing a large size effect but over a very small indentation depth range.

The concept of relaxation of strain energy over a volume by the introduction of a dislocation is well known from the Matthew's critical thickness in strained layer growth. In this situation the critical strain that can be sustained without relaxation is

$$\varepsilon_c \approx \frac{b}{h_c} \qquad (3)$$

where b is the magnitude of the Burger's vector of the dislocation and h_c is the critical thickness of the layer.

Now the strain at yield is

$$\varepsilon_y = \varepsilon_c + \varepsilon_0 \qquad (4)$$

where ε_0 is the macroscopic yield strain.

If the radius of the smallest volume that can begin to relax is proportional to r, then from critical thickness theory we have,

$$\varepsilon_y \approx \frac{b}{r} + \varepsilon_0 \qquad (5)$$

or

$$\sigma_y \approx \frac{Eb}{r} + \sigma_0 \qquad (6)$$

where E is an appropriate modulus and σ_0 is the macroscopic yield stress.

In the case of the four metals investigated here, the value of ε_0 is similar for all the metals and the size effect is dominated by the geometrical ε_c term. In strained layer growth, r is simply the layer thickness. In a strain gradient, such as a thin beam in flexure or a thin wire in torsion, the dimension r is a position within the strain gradient found by integrating the strain over the gradient [15]. From the experimental results,

$$\frac{Eb}{r} \approx \sigma_0 \left[\left(\frac{\sigma_y}{\sigma_0} \right) - 1 \right] = \frac{k\sigma_0}{R^{1/3}} \qquad (7)$$

where k is a constant determined from the slope of Figure 2, implying that

$$\frac{r^3}{R} \approx \left(\frac{Eb}{k\sigma_0} \right)^3 \qquad (8)$$

that is, the yield stress is proportional to a volume.

5. Conclusions

A key conclusion from this work is that the plasticity size effect is related to dislocation generation rather than to interaction. The fact that the relative increase in yield stress required to simulate the experimental data is the same for all of the materials tested, independent of grain size and spanning a wide range of materials properties, implies that a geometric effect, linked to the stress distribution under the indenter, is responsible. The increase in the elastic limit is consistent with the argument that as an imposed elastic strain becomes increasingly localised, a higher force will be required to satisfy the energetic yield criteria when integrated over the effective volume of material affected by the generation of a dislocation. The implications of this are profound. The relation obtained here may be used to predict the increased resistance of materials to small radius contacts. Further, by induction, it is clear that for any particular material, the size effect can be extracted to leave a size independent relationship between the indentation imposed true stress and true strain that is directly equivalent to the uniaxial stress-strain curve. Thus, using this method to account for the indentation size effect, it should be possible to predict uniaxial tensile properties by spherical indentation of bulk materials. Furthermore, it is predicted that if any dimension of a material compromises the effective volume of yield, then a further enhancement of yield stress should be expected. Thin layers or multi-layers will therefore exhibit both increased hardness and toughness since the yield stress can be engineered to be higher without losing the ductile properties of the material. In principle, material independent design rules for such property enhancement are attainable by suitable identification of the relationship between finite volume for yield (or more usefully radius of the contact) and material properties such as elastic modulus and yield stress.

Acknowledgements

The support of EPSRC and NPL (Industrial CASE award) and the UK Department of Trade and Industry are acknowledged. We thank Prof. D.J.Dunstan for useful discussions.

References

1. D. Tabor, *The Hardness of Metals* (Clarendon Press, Oxford, 1951).
2. A.J.Bushby and N.M.Jennett, Mater. Res. Soc. Symp. Proc., **649** (2001) Q7.17.1
3. N.M.Jennett, G.Shafirstein and S.R.J.Saunders, Proc. 9th Int. Symp. Hardness Testing in Theory and Practice. Düsseldorf Nov 1995, VDI Berichte **1194** pp201-210 (Publ. VDI-Verlag GmbH, Dusseldorf, 1995).
4. A.J.Bushby and D.J.Dunstan, J. Mater. Res. **19** 137 (2004).
5. W.D. Nix, and H. Gao, J. Mech. Phys. Solids **46** 411 (1998).
6. W.W. Gerberich, J.C. Nelson, E.T. Lilleodden, P. Anderson and J.T. Wykobek, Acta Mater. **44** 3585 (1996).
7. D.F. Bahr, D.E. Krammer and W.W. Gerberich, Acta Mater. **46** 3605 (1998).
8. Y.Y. Lim and M.M.Chaudhri, Philos. Mag. **A79** 2979 (1999).
9. Y.Y. Lim, A.J. Bushby and M.M. Chaudhri, Mater. Res. Soc. Symp. Proc. **522** 145 (1998)
10. Y.Y. Lim, PhD thesis, 'Nanoindentation hardness studies of metallic surfaces and thin films' Trinity College, Cambridge (2000).
11. J.G. Swadener, E.P. George and G.M. Pharr, J. Mech. Phys. Solids **50** 681 (2002).
12. N.B. Jayaweera, J.R. Downes, M.D. Frogley, M. Hopkinson, A.J. Bushby, P.Kidd, A. Kelly and D.J. Dunstan, Proc. Roy. Soc. **A459** 2049 (2003).
13. E.A. Fitzgerald, Material Science Reports **7** 87 (1991).
14. D.J Dunstan, J. Mater. Sci.: Mater. Elect. **8** 337 (1997).
15. D.J.Dunstan and A.J.Bushby, Proc. Roy. Soc. **A460** 2781 (2004).
16. I.Spary, A.J.Bushby, N.M.Jennett and G.M.Pharr, Mater. Res. Soc. Symp. Proc. **778**, 123 (2003).

17. S.Qu, Y.Huang, G.M.Pharr and K.C.Hwang, Int. J. Plast. **22** 1265 (2006).

18. Y.Huang, S.Qu, K.C.Hwang, M.Li and H. Gao, Int. J. Plast. **20** 753 (2004).

19. Y.Choi, K.J. Van Vliet, J.Li and S.Suresh, J.Appl. Phys. **94** 6050 (2003).

20. M.Uchic, D.M.Dimiduk, J.N.Florando and W.D.Nix, Science **305** 986 (2004).

21. P. Moreau, M. Raulic, K.M.Y. P'ng, G. Gannaway, P. Anderson, W.P. Gillin, A.J.Bushby and D.J. Dunstan, Philos. Mag. Letts. **85** 339 (2005).

22. H.D.Espinosa, S.Berbenni, M.Panico and K.W.Schwarz, PNAS **102**(47) 16933 (2005).

23. W.D.Nix, J.R.Greer, G.Feng and E.T.Lilleodden, Thin Solid Films, in press (2006).

24. C.Zhang and G.Xu, Mater. Sci. Eng. A. **400-401** 471 (2005).

25. M.F.Horstemeyer and M.I.Baskes, ASME J. Eng. Technol., **121** 114 (1999)

26. W.W.Gerberich, N.I.Tymiak, J.C.Grunlan, M.F.Horstemeyer and M.I.Baskes, J. Appl. Mech., **69** 433 (2002).

27. I. Spary, N.M. Jennett, A.J.Bushby, Mater. Res. Soc. Symp. Proc. **795** U10.6.1-6 (2004).

Deleted: ¶

Table 1. Material properties. Grain size determined by optical metallography. Burgers vector calculated as lattice parameter / √2. σ_0 is the yield stress determined in the uniaxial test.

Metal	grain size /μm	*E* / GPa	*G* / GPa	σ_0 / MPa	σ_0/G $\times 10^{-3}$	*b* / nm	Stacking fault energy / mJ m^{-2}
Al	330 ± 40	69	26.5	11	0.42	0.286	135
Cu	70 ±30	118	43.9	13	0.30	0.256	41
Ni	45 ±15	220	78.6	78	0.99	0.249	240
Ir	30	510	202	109	0.54	0.272	-

Table 2. Values of yield stress, in MPa used in the FE simulations, ± limits on possible values that might be considered a fit to the experimental data.

	Al	Cu	Ni	Ir
Uniaxial	11	13	78	109
R / μm				
1600				220 ± 60
500		15 ± 5		
318				220 ± 60
290			348 ± 30	
200	22 ± 4	15 ± 5		
122				400 ± 120
69				550 ± 100
30	57 ± 4	59 ± 12		
20			436 ± 13	
14				637 ± 80
10			495 ± 12	
7	81 ± 6	92 ± 10		
5			592 ± 20	

Figure 1. Experimental indentation data (open symbols), FE simulation (closed symbols), FE simulation using uniaxial data directly (crosses), Tabor representation of uniaxial data (solid lines), Hertzian elastic response (dashed line).

a) Aluminium: circle, R = 200μm; square, R = 30μm; diamond R = 7μm.
b) Copper: square, R = 500μm; circle, R = 200μm; triangle, R = 30μm; diamond R = 7μm.
c) Nickel: circle, R = 290μm; triangle, R = 20μm; square, R = 10μm; diamond R = 5μm.
d) Iridium: grey circle, R = 1600μm; open circle, R = 318μm; diamond R = 122μm; triangle, R = 69μm; square, R = 14μm. Error bars show likely uncertainty in data based on description in [11].

Figure 2. The yield stress required to simulate the size effect normalised by the uniaxial yield stress for all metals studied, as a function of (a) $1/R^{1/3}$ and (b) $1/R^{1/2}$, for: Aluminium (diamond); Copper (square); Nickel (triangle); Iridium (circle). The data are normalised by the uniaxial yield stress for each metal tested, so that the uniaxial yield stress is plotted on the ordinate at a value of unity. The solid line is a linear regression to all the data with the intercept at the normalising value of unity. The dashed line is a free regression fit to the data from smaller radius indenters (R< 30μm) with the least uncertainty.

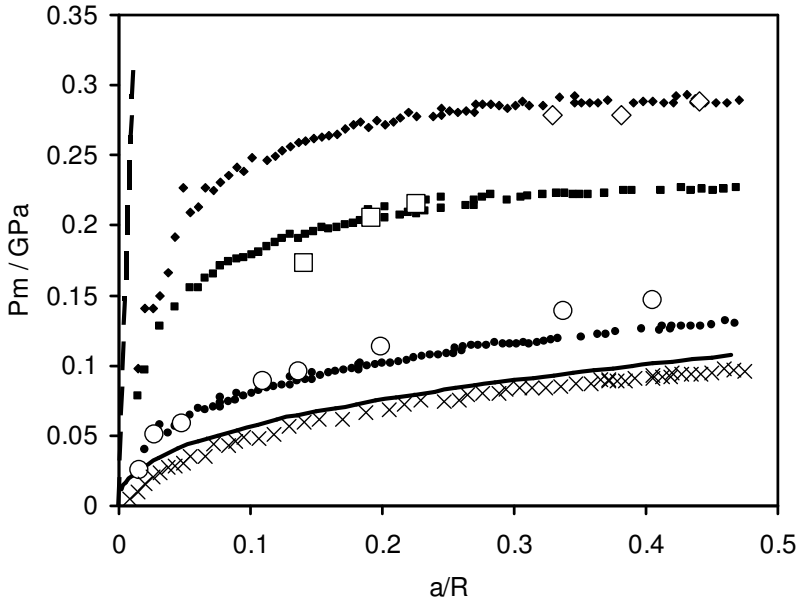

Figure 1a

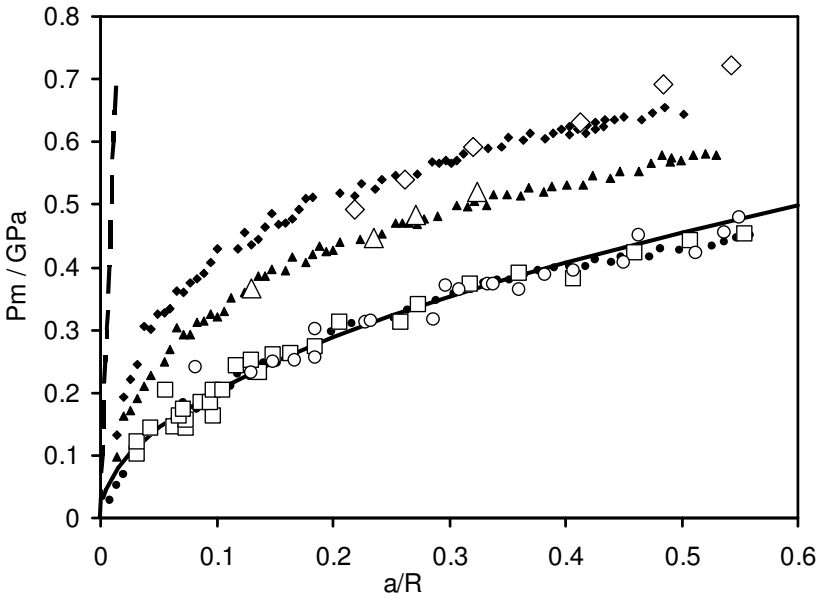

Figure 1b

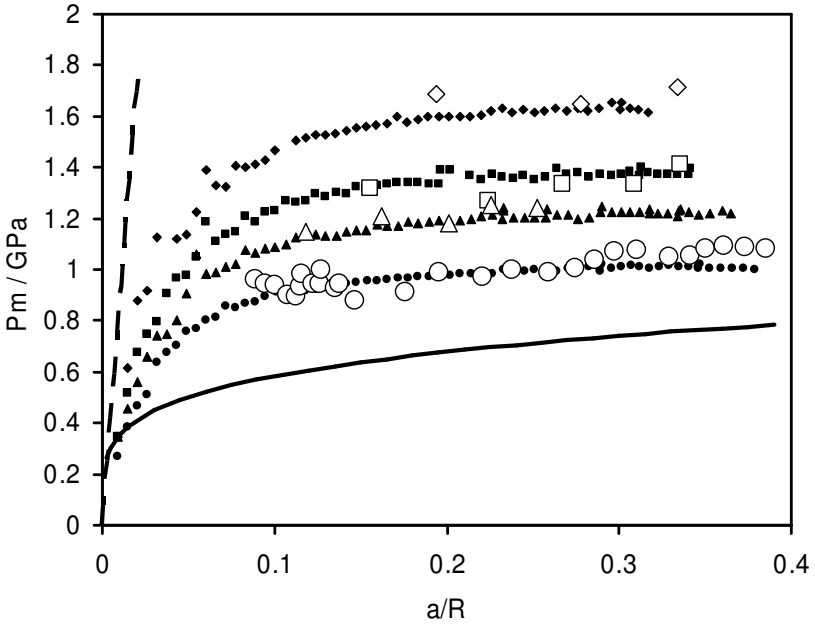

Figure 1c

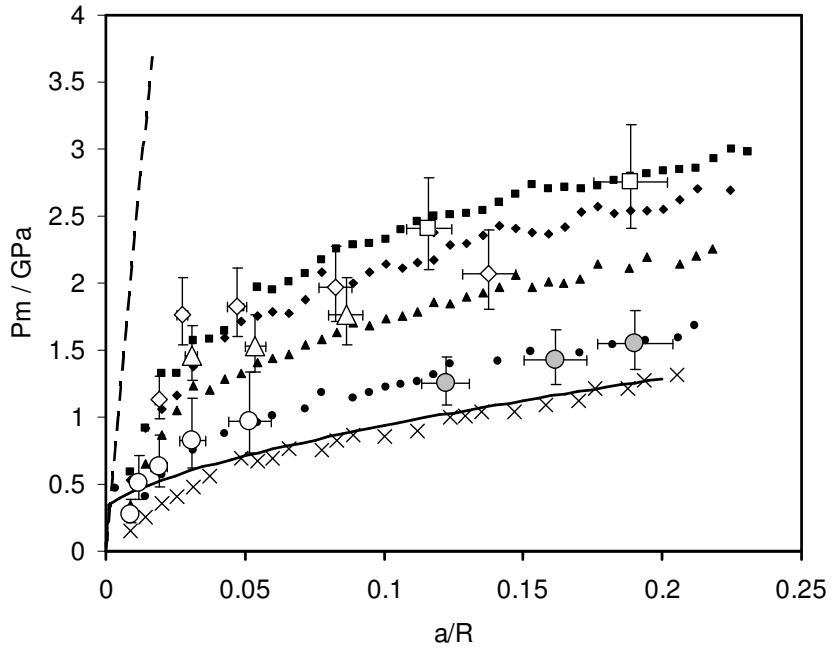

Figure 1d

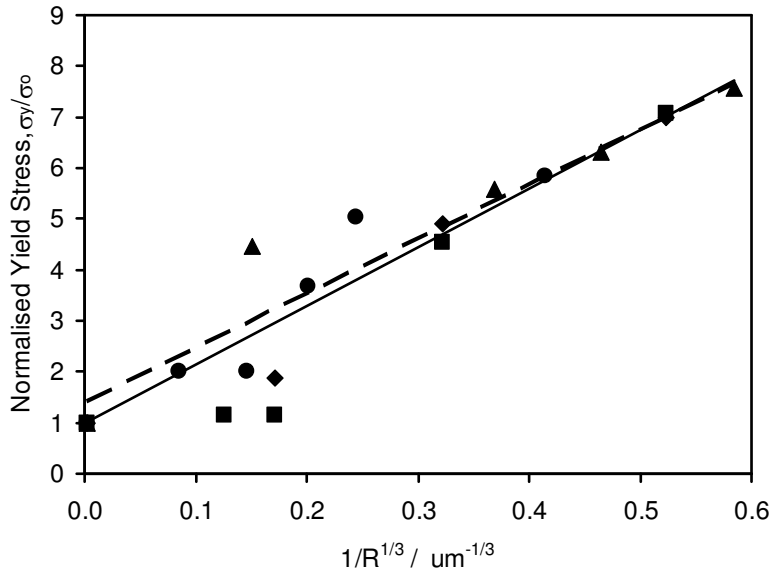

Figure 2a

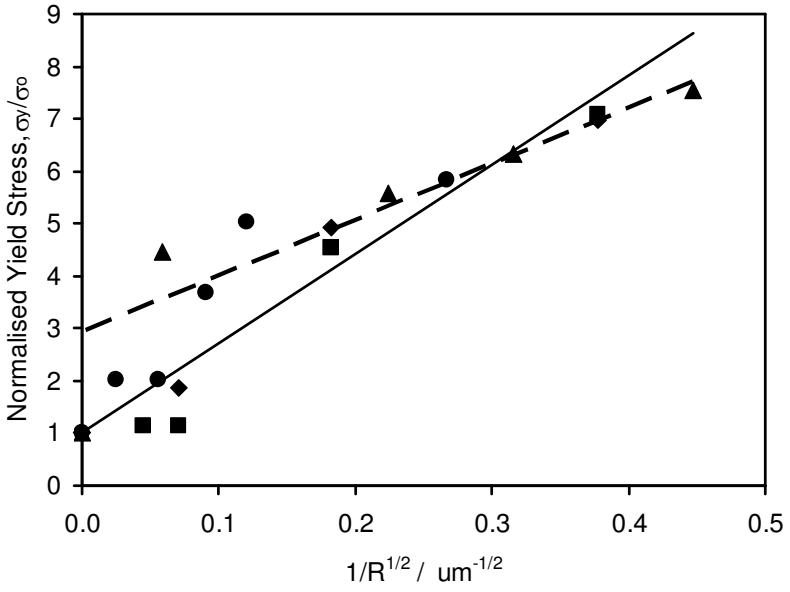

Figure 2b